Dalton Transactions

PAPER

View Article Online
View Journal | View Issue

Cite this: *Dalton Trans.*, 2017, **46**, 14638

Clinical evaluation of the radiolanthanide terbium-152: first-in-human PET/CT with ^{152}Tb-DOTATOC

Richard P. Baum, †[a] Aviral Singh,*†[a] Martina Benešová,[b,c] Christiaan Vermeulen,[b] Silvano Gnesin,[d] Ulli Köster,[e] Karl Johnston,[f] Dirk Müller,[a] Stefan Senftleben,[a] Harshad R. Kulkarni,[a] Andreas Türler,[g,h] Roger Schibli,[b,c] John O. Prior,[d] Nicholas P. van der Meulen[b,g] and Cristina Müller*[b,c]

The existence of theragnostic pairs of radionuclides allows the preparation of radiopharmaceuticals for diagnostic and therapeutic purposes. Radiolanthanides, such as ^{177}Lu, are successfully used for therapeutic purposes; however, a perfect diagnostic match is currently not available for clinical use. A unique, multi-disciplinary study was performed using ^{152}Tb ($T_{1/2}$ = 17.5 h, $E\beta^+_{average}$ = 1140 keV, $I\beta^+$ = 20.3%), which resulted in the first-in-human PET/CT images with this promising radionuclide. For this purpose, ^{152}Tb was produced *via* a spallation process followed by mass separation at ISOLDE, CERN. The chemical separation and quality control, performed at PSI, resulted in a pure product in sufficient yields. Clinical PET phantom studies revealed an increased image noise level, because of the smaller β^+ branching ratio of ^{152}Tb as compared to standard PET nuclides at matched activity concentrations; however, the expected recovery would be comparable at matched signal-to-noise ratios in clinical PET. ^{152}Tb was used for labeling DOTATOC, at Zentralklinik Bad Berka, and administered to a patient for a first-in-human clinical study. PET scans were performed over a period of 24 h, allowing the visualization of even small metastases with increased tumor-to-background contrast over time. Based on the results obtained in this work, it can be deduced that PET/CT imaging with ^{152}Tb-labeled targeting agents has promise for clinical application and may be particularly interesting for pre-therapeutic dosimetry.

Received 27th May 2017,
Accepted 7th August 2017

DOI: 10.1039/c7dt01936j

rsc.li/dalton

Introduction

The existence of theragnostic pairs of radionuclides of the same element allows the preparation of chemically identical radiopharmaceuticals for diagnostic and therapeutic purposes. In this regard, radioiodine presents an excellent example, as it has been used successfully to diagnose ($^{123/124}$I) and treat (^{131}I) differentiated thyroid cancer for several decades.[1] Indeed, this was the first theragnostic application of matched radionuclides in nuclear medicine. When utilizing radionuclides in combination with targeting agents, radiometals are commonly preferred over radioiodine due to the increased *in vivo* stability and an easy preparation of defined radioconjugates.[2] There are a number of radiometals potentially useful for radiotheragnostics; among those are matched pairs of yttrium (^{86}Y/^{90}Y), copper (^{64}Cu/^{67}Cu), scandium ($^{43/44}$Sc/^{47}Sc) and lead (^{203}Pb/^{212}Pb).[3–10]

At Paul Scherrer Institut (PSI), research endeavors in recent years have focused on the investigation of terbium radionuclides.[11] Terbium, a lanthanide, is unique in that it presents four medically interesting radionuclides, for SPECT (^{155}Tb) and PET (^{152}Tb) imaging purposes and for α-therapy (^{149}Tb) and β^-/Auger-e^- therapy (^{161}Tb).[11] Interest has been shown in ^{161}Tb, which has similar physical properties to ^{177}Lu and, in addition, emits a substantial number of Auger/conversion

[a]*THERANOSTICS Centre for Molecular Radiotherapy and Molecular Imaging, ENETS Center of Excellence, Zentralklinik Bad Berka, Germany. E-mail: aviral.singh@zentralklinik.de; Fax: +49 364 585-3515; Tel: +49 364 585-42226*
[b]*Center for Radiopharmaceutical Sciences ETH-PSI-USZ, Paul Scherrer Institut, Villigen-PSI, Switzerland. E-mail: cristina.mueller@psi.ch; Fax: +41 56 310 28 43; Tel: +41 56 310 44 54*
[c]*Department of Chemistry and Applied Biosciences, ETH Zurich, Zurich, Switzerland*
[d]*Department of Nuclear Medicine and Molecular Imaging, Lausanne University Hospital, Lausanne, Switzerland*
[e]*Institut Laue-Langevin, Grenoble, France*
[f]*ISOLDE/CERN, Meyrin, Switzerland*
[g]*Laboratory of Radiochemistry, Paul Scherrer Institut, Villigen-PSI, Switzerland*
[h]*Department of Chemistry and Biochemistry, University of Bern, Bern, Switzerland*
† These authors contributed equally to this manuscript.

electrons.[12] De Jong *et al.* reported on the favorable physical characteristics of ^{161}Tb and presented *in vitro* and *in vivo* studies performed with ^{161}Tb-labeled DTPA-octreotide in tumor-bearing rats.[13] Preclinical therapy studies performed at PSI demonstrated the superiority of ^{161}Tb over ^{177}Lu, which was attributed to the co-emission of Auger electrons.[14,15] Additional side effects to the kidneys were not observed.[16] Theoretical calculations of the absorbed radiation dose in spheres of different diameters revealed that ^{161}Tb can effectively irradiate isolated tumor cells and micrometastases, due to its decay spectrum combining β^--particles of medium energy and Auger electrons.[17,18] These promising characteristics warrant clinical investigation using ^{161}Tb, when steady supply in sufficient quantities can be guaranteed.

A diagnostic match to therapeutic radiolanthanides is currently not available for clinical use. ^{68}Ga-labeled DOTATOC and DOTATATE are, however, used routinely for the imaging of somatostatin receptor-positive neuroendocrine neoplasms, prior to peptide receptor radionuclide therapy (PRRT) using ^{177}Lu- or ^{90}Y-labeled somatostatin analogues.[19–22] While the use of the radiometal ^{68}Ga is considered a success in diagnostic applications, this positron-emitting nuclide is not suitable for pre-therapeutic dosimetry estimations due to its short half-life of only 68 min.

The use of ^{152}Tb may be a solution to address this issue. It decays with a half-life of 17.5 h by the emission of positrons ($E\beta^+_{average}$ = 1140 keV, $I\beta^+$ = 20.3%) without the emission of α- or β^--particles, but by the co-emission of several γ-rays (Table 1). It would, thus, be an exact diagnostic match to ^{161}Tb and ^{149}Tb, as well as to other therapeutic radiolanthanides, including ^{177}Lu.[23] The current availability of ^{152}Tb is scarce. The nuclide can be produced, however, by proton-induced spallation and on-line mass separation, followed by chemical separation, as previously reported and exemplified at the ISOLDE facility at CERN, Switzerland.[11,23,24] An initial proof-of-concept study was performed with ^{152}Tb-labeled folate in a mouse bearing folate receptor (FR)-positive tumors.[11] A more extensive *in vivo* imaging study demonstrated the potential of ^{152}Tb-labeled DOTANOC for the PET/CT imaging of AR42J tumor-bearing mice.[23]

The aim of the present study was, therefore, to investigate ^{152}Tb in a clinical proof-of-concept PET/CT study. For this purpose, ^{152}Tb was produced at the ISOLDE facility (CERN, Geneva, Switzerland), and was separated from the collection matrix and impurities at PSI. Phantom studies were performed with a clinical PET/CT scanner at Lausanne University Hospital (Centre Hospitalier Universitaire Vaudois or CHUV), Switzerland, and at Zentralklinik Bad Berka (ZBB), Germany, in order to determine the image quality and investigate the possibility of ^{152}Tb-based PET quantification. Finally, DOTATOC was labeled with ^{152}Tb at ZBB's radiopharmacy, and used for a first-in-human clinical PET/CT study.

Table 1 Decay properties of ^{152}Tb based on NuDat 2.6 (http://www.nndc.bnl.gov/nudat2/)

Radionuclide	Half-life	$E\beta^+_{average}$ (I)	Significant γ-rays (I > 5%), Eγ (I)
^{152}Tb	17.5 h	1140 (20.3%)	271 (9.53%) 344 (63.5%) 586 (9.21%) 779 (5.54%)

Table reproduced from Müller *et al.*, EJNMMI Res., 2016.[23]

Experimental

Production of terbium-152 (^{152}Tb)

^{152}Tb was produced through 1.4 GeV proton-induced spallation in a tantalum target (55 g cm^{-2}) at ISOLDE (CERN, Geneva, Switzerland). The spallation products were released online from the hot (~2000 °C) target and ionized in a hot (~2000 °C) tungsten ionizer. The cumulative ^{152}Tb yields were significantly boosted by the resonant laser ionization of the radioactive precursor, ^{152}Dy.[25] The ions were then accelerated to 30 keV and mass-separated, as previously reported.[11,23,24] Ions of mass 152 were implanted into zinc-coated gold foils over a collection period of, typically, 4 hours. The collected samples were allowed to stand, to allow most of the short-lived ^{152}Dy ($T_{1/2}$ = 2.4 h), as well as the even shorter lived ^{136}Nd and ^{136}Pr oxides collected at the same mass setting (136 + 16 = 152), to decay. The samples were then transported over a distance of 270 km from CERN to PSI.

Separation of ^{152}Tb from the collection matrix and quality control of the product

The zinc layer containing ^{152}Tb and impurities of mass 152 (^{152}Dy and ^{152}Gd) and 136 (^{136}Nd/^{136}Pr oxides) was dissolved in 0.1 M HNO_3/NH_4NO_3 at 80 °C. After the addition of H_2O, the dissolved zinc layer, along with the radionuclidic implants, was passed through a 50 mm × 5 mm column containing a macroporous strongly acidic cation exchange resin, as previously reported.[11] A concentration gradient of α-hydroxyisobutyric acid (α-HIBA, pH 4.7) ranging from 0.07 to 0.13 M was used for elution. The gradient pump was set to run at 0.6 mL min^{-1} and reduced to 0.4 mL min^{-1} after 30 min, when fractions of 1 mL were collected in pre-washed Eppendorf tubes. Small samples (10 μL) were taken from the fractions containing the most activity and measured using an N-type high-purity germanium coaxial detector (EURISYS MESURES, France).

For the patient study to be performed at ZBB, the radioactive solutions of the fractions with the highest activity were combined and evaporated to dryness by heating the solution to 80 °C for 1 h, followed by 15 min at 100 °C. The activity was subsequently dissolved in 0.05 M HCl (30% Suprapur, Merck KGaA, Germany). Quality control of the ^{152}Tb product was performed by analyzing the labeling of DOTANOC using analytical high performance liquid chromatography (HPLC), performed on a Merck–Hitachi system, and a radiometric detector. The peptide (DOTANOC acetate, ABX GmbH) was dissolved in

Milli-Q water to obtain a stock solution of 1 mM. A mixture of ^{152}Tb in 0.05 M HCl (20 μL), 0.05 M HCl (30 μL), 0.5 M sodium acetate (10 μL, pH 8) and DOTANOC solution (2.4 μL, 1 mM, corresponding to 2.4 nmol) was incubated for 10 min at 95 °C. Afterwards, a 5 μL sample of the labeling solution was diluted with Milli-Q water and injected into an HPLC system equipped with a reversed-phase column (Xterra™, MS, C18, 5 μm, 150 × 4.6 mm; Waters). The mobile phase consisted of Milli-Q water containing 0.1% trifluoroacetic acid (A) and acetonitrile (B). A gradient from 95% A and 5% B to 20% A and 80% B over a period of 15 min was used at a flow rate of 1.0 mL min^{-1}.

PET/CT study of a NEMA NU2 phantom

After chemical separation at PSI, ^{152}Tb (~150 MBq) was shipped to Lausanne, where it was used for a phantom study at the Nuclear Medicine and Molecular Imaging Department at CHUV. For this purpose, a standard NEMA NU2 phantom composed of a main volume of 9.34 L and six spherical inserts with diameters of 10 mm, 13 mm, 17 mm, 22 mm, 28 mm and 37 mm, respectively, was employed to assess recovery coefficients (RC) in spherical inserts as a function of the insert size. A lung insert was also available for this phantom and was used to estimate the relative lung error (ΔC_{lung}). The ^{152}Tb solution was diluted to obtain an activity of 1.8 MBq in 200 mL (activity concentration: 9.0 kBq mL^{-1}) to fill the phantom spheres. An activity of 11.2 MBq in 9.34 L (activity concentration: 1.2 kBq mL^{-1}) was used to fill the main phantom volume, in order to obtain a ratio of 7.5 : 1 between the activity concentrations in the spheres and background volume, respectively.

A 10-min list-mode time-of-flight (TOF) PET/CT acquisition was performed with a GE Discovery D690 TOF PET/CT scanner (GE Healthcare, Waukesha, WI).[26] Two reconstructions with three iterations and 21 subsets were performed using the vendor's ordered-subset expectation maximization (OSEM) algorithm. The first reconstruction included TOF and resolution recovery corrections (GE-VPFXS) with a post-reconstruction Gaussian filter with a full width at half maximum (FWHM) of 5 mm while the second reconstruction, without TOF and PSP (GE-VPHD), employed a Gaussian filter with a FWHM of 7 mm. The reconstructed field of view had a diameter of 70 cm and a matrix size of 256 × 256, with a slice thickness of 3.27 mm. The CT scan was acquired at 120 kV, 0.8 second gantry rotation time, tube current of 113 mA and a pitch of 1.375. The CT field of view was 70 cm with a matrix size of 512 × 512 and a slice thickness of 3.7 mm.

The PET acquisition was performed with the standard whole-body ^{18}F setup. Direct absolute quantification for ^{152}Tb was not possible, since a specific prompt-gamma correction for this radionuclide was not available. A relative quantification was performed by rescaling the measured average activity concentration in the phantom background to the expected activity concentration, according to the phantom preparation. Average and maximum voxel relative recovery coefficients (RC), as a function of the insert size, were computed by placing a spherical volume of interest (VOI) on each insert and measuring the mean voxel value in the VOI defined by a 3D isocontour at 50%, adapted for background as previously defined[27] and the maximum value of the activity concentration divided by the expected activity concentration known from the phantom preparation. According to the NEMA NU2 procedure,[28] the relative error in the lung insert was defined by:

$$\Delta C_{\mathrm{lung}}\,(\%) = \frac{a_{\mathrm{c,lung}}}{A_{\mathrm{c,bg}}} \times 100$$

where $a_{\mathrm{c,lung}}$ is the average activity concentration measured in a cylindrical VOI of 3 cm in diameter and 16 cm in length, placed in the lung insert, and $A_{\mathrm{c,bg}}$ is the expected background activity concentration known from the phantom preparation. The image noise was evaluated by the coefficient of variation (COV), defined as the ratio between the standard deviation and the average signal measured from the phantom background.

Radiolabeling of DOTATOC

A solution of ^{152}Tb in 0.05 M HCl (450 μL, 551 MBq) was prepared at PSI and transported to ZBB. Ten hours after preparation, ^{152}Tb radioactivity was used for the radiolabeling of DOTATOC, as previously reported by Müller *et al.*[23] In brief, DOTATOC (150 μg) was labeled with ^{152}Tb (343 MBq) using a solution of 7.7 mg gentisic acid in 0.4 M sodium acetate buffer (700 μL, pH 4.6). The reaction mixture was incubated at 95 °C for 40 min. Quality control was performed using analytical HPLC (a Jasco PU-1580 system) equipped with a radiometric detector and a reversed-phase column (Jupiter™ Proteo 90 Å, LC, C-18, 4 μm, 250 × 4.6 mm, Phenomenex). The mobile phase consisted of Milli-Q water containing 5% acetonitrile and 0.1% trifluoroacetic acid (A) and acetonitrile containing 0.5% Milli-Q water and 0.1% trifluoroacetic acid (B). The gradient from 100% A to 100% B over a period of 15 min was used, at a flow rate of 1 mL min^{-1}. The reaction solution was diluted with 1 mL sterile 0.9% saline and filtered using a 0.2 μm sterile filter. Samples were taken for sterility and endotoxin testing using an Endosafe®-PTS™ cartridge. The pH value of the final product was then determined.

Patient selection and regulatory issues

In accordance with the German Medicinal Act (section 13, subsection 2b), the responsible regulatory authority of the state, Government of Thuringia, and the 1964 Declaration of Helsinki, ^{152}Tb-DOTATOC was administered to a 67-year-old patient with metastatic well-differentiated functional neuroendocrine neoplasm of the ileum, presenting for restaging 8 years after the sixth cycle of PRRT (Table 2). An institutional review board (European Neuroendocrine Tumor Society certified tumor board) approved the study, which was performed in compliance with the regulations of the German Federal Agency for Radiation Protection. Since this was not a formal clinical trial, but a retrospective report on findings obtained within routine clinical care, a formal approval by an ethics committee was not required. The patient signed a substantial written informed consent prior to the investigation and, in addition, he provided signed consent concerning the collection and

Table 2 Patient characteristics, history of the disease and clinical data

Characteristics	Details
Age	67 years
Gender	Male
Diagnosis	Metastatic, well-differentiated, functional neuroendocrine neoplasm of the terminal ileum
Metastases	Liver, lymph nodes, peritoneum, pancreatic head, intramuscular, pericardium
Current disease status	Stable disease
Ki-67 of primary tumor	<5%
Functionality	Serotonin secretion, carcinoid syndrome
Karnofsky Performance Score (at the time of this study)	100%
PRRT schedule:	Cumulative activity administered:
May 2005 until October 2007 ^{90}Y-DOTATATE (n = 5)	15.2 GBq (^{90}Y-DOTATATE)
June 2008 ^{177}Lu-DOTATATE (n = 1)	7.5 GBq (^{177}Lu-DOTATATE)
Relevant previous surgery	Partial resection of ileum
Last restaging with PET/CT	June 2015: ^{68}Ga-DOTATOC PET/CT
Clinical indication	Restaging 8 years after the 6th PRRT cycle

storage of the clinical data in the institutional database and national registry as well as the anonymized evaluation and publication of these data.

PET/CT acquisition protocol

PET/CT imaging was performed using a Biograph mCT Flow 64 scanner (Siemens Medical Solutions AG, Erlangen, Germany). Whole-body PET/CT scans were acquired in the supine position from the vertex to the feet at various time intervals. The PET scans were acquired using speeds of 1.1 and 0.8 mm s^{-1} (for later time points) in flow-motion, which is similar to 2 min per bed or 2.5 min per bed in the stop-and-go acquisition mode. The reconstruction was performed using recon TrueX + ToF with 3 iterations and 21 subsets. The images were reconstructed using a Gaussian filter (2 mm FWHM) and a matrix size of 200 × 200. The CT scans were acquired at 100 kV and at a pitch of 1.5. CareDose4D was applied using a 0.5 second gantry rotation time, 5 mm slice thickness and a matrix size of 512 × 512.

PET/CT imaging of a patient using ^{152}Tb-DOTATOC

As part of the routine restaging procedure, blood samples from the patient were sent to the institutional laboratory for analysis. The patient received a bolus intravenous injection of 145 MBq of ^{152}Tb-DOTATOC (2.5 MBq kg^{-1}) in May 2016. No intravenous or oral contrast was given, due to reduced renal function. Four sets of whole-body PET/CT scans of the patient were acquired over two consecutive days. The time points of image acquisition were 25 min, 2 h, 17 h, and 24 h after injection of the radiopharmaceutical, respectively.

Analysis of the human PET/CT images

The PET/CT images obtained using ^{152}Tb-DOTATOC were interpreted independently by two physicians (one board-certified nuclear medicine physician and one board-certified radiologist, each with over ten years of experience in reporting PET/CT studies with somatostatin analogues). A qualitative evaluation of the scans was performed by analyzing the biodistribution of the radiopeptide, along with uptake in the somatostatin receptor (SSTR)-expressing lesions on the whole-body, transverse, coronal and sagittal images. The PET/CT images were compared with those obtained using ^{68}Ga-DOTATOC 11 months previously. Semi-quantitative evaluation using SUV was, however, not performed for this initial study.

Results

Production of ^{152}Tb

Due to efficient resonant laser ionization, the ratio between ^{152}Dy and ^{152}Tb was greater than 20 : 1 during collection, which means that the mass number 152 isobars consisted of more than 95% ^{152}Dy and less than 5% of ^{152}Tb. Multi reflection time-of-flight mass spectrometer analysis[29] showed that the unwanted isobars, namely, ^{152}Gd and ^{152}Eu, occurred to a lesser extent by about 2 orders of magnitude than ^{152}Dy and ^{152}Tb in terms of atomic ratio (*i.e.* 1 × 10^{-6} in terms of the activity ratio for ^{152}Eu/^{152}Tb) before chemical separation. Moreover, the atomic ratio of ^{136}Nd/^{136}Pr oxides to all isobar nuclides of mass number 152 was less than 1 × 10^{-5}, and the activity ratio of ^{136}Nd/^{136}Pr oxides to ^{152}Tb was less than 2 × 10^{-4} at the time of arrival at PSI, decaying to negligible levels before final use. As a result, ^{152}Gd, ^{152}Eu and ^{136}Nd/^{136}Pr could be safely neglected, even if they were not fully separated from ^{152}Dy/^{152}Tb.

Radiochemical purification of ^{152}Tb

The radiochemical separations were performed typically between 12 and 16 hours after the end of collection. The total measured radioactivity at the beginning of the separation contained about 10% of ^{152}Dy. The gradient elution of the column at low pump speeds ensured the clean elution of ^{152}Tb, together with ^{152}Dy, leaving the remaining contaminants to be eluted with more concentrated solutions afterwards. The eluted fractions containing the highest activities of ^{152}Tb/^{152}Dy were selected and combined to obtain about 675 MBq of ^{152}Tb in ~1.5 mL of α-HIBA. γ-Spectra taken just after separation confirmed the presence of both ^{152}Tb and ^{152}Dy in the final product. The analysis of the ^{152}Tb solution the day after production revealed a radiochemically pure product as, by this time, all the ^{152}Dy had decayed to ^{152}Tb.

As part of the first-in-human study, the ^{152}Tb solution was processed further to ensure high quality radiolabeling. After evaporation of the eluted ^{152}Tb solution and reconstitution in 0.05 M HCl, the ^{152}Tb activity was used for the labeling of DOTANOC at a specific activity of 10 MBq nmol^{-1}. The quality control performed, using HPLC, revealed a radiochemical

purity of >98%. Having confirmed the excellent quality of the radionuclide, a solution containing about 500 MBq ^{152}Tb was shipped over a distance of ~600 km from PSI to ZBB.

As a part of a second experiment, a sample of ~150 MBq ^{152}Tb in α-HIBA was shipped the morning after separation, from PSI to CHUV, for the performance of human phantom studies.

Phantom studies

The transaxial view of the NEMA NU2 phantom is shown in Fig. 1A. For both reconstructions, the background variability measured by COV was 25%. The relative maximum and average (50%) recovery coefficients for each spherical insert are shown in Fig. 1B and C. The OSEM3D TOF + PSF reconstruction exhibited maximum and average RC values comparable to the RC reported in the literature for ^{18}F PET reconstructions using TOF and point spread function (PSF) corrections.[30] Lower RC values were obtained with the simple OSEM3D reconstruction. Relative lung errors were 12.2% and 40.2% for the OSEM3D TOF + PSF and OSEM3D reconstruction, respectively. These results have been confirmed by an independent phantom experiment performed in the Siemens Biograph mCT Flow 64 PET/CT device at ZBB (data not shown).

Preparation of ^{152}Tb-DOTATOC for human use

The radiochemical purity of the final product, performed at ZBB, was >97%, thereby allowing its application without any further purification. The pH value of the final product was 4.6, while the bacterial endotoxin test was negative. Due to the small application volume (<3 mL), it was not necessary to determine and adjust the osmolarity of the final product. The specific activity of the sterile-filtered and applied product (145 MBq) was 1.37 MBq nmol^{-1}, calculated for 150 μg DOTATOC.

PET/CT imaging studies of a patient

PET/CT images were obtained from a 67-year-old patient with metastatic well-differentiated functional neuroendocrine neoplasm of the ileum, presenting for restaging 8 years after the sixth cycle of PRRT (Fig. 2). The biodistribution of ^{152}Tb-DOTATOC was assessed visually using PET/CT slices acquired at four different time-points on two subsequent days (Fig. 2). The early images performed at 25 min after injection demonstrated uptake in the blood pool, soft tissue, kidneys, and in some lymph node metastases. Moderate-to-low tracer uptake in the liver and spleen was also visualized. Renal excretion of ^{152}Tb-DOTATOC was seen by tracer uptake in the kidneys, the pelvicalyceal system and the urinary bladder. At 2 h after injection, radioactivity was still seen in the blood pool and soft tissue; however, the uptake in the liver, spleen, as well as in lymph node and skeletal metastases was increased. Renal excretion continued, with increasing activity detectable in the urinary bladder. At 17 h after injection of ^{152}Tb-DOTATOC, the tracer was no longer visible in the blood vessels. The uptake was more prominent in SSR-expressing organs, such as the pituitary gland (comparatively moderate-to-low uptake), the spleen, and in multiple SSR-expressing lymph node and skeletal metastases. Very low uptake was present in the shoulders due to inflammatory/degenerative changes. Persistent renal uptake was visible in the kidneys along with urinary bladder activity. Some activity was also detected in the intestines as a consequence of the elimination of ^{152}Tb-DOTATOC. On the delayed images at 24 hours after injection, physiological uptake of the radiopeptide was present in the pituitary gland,

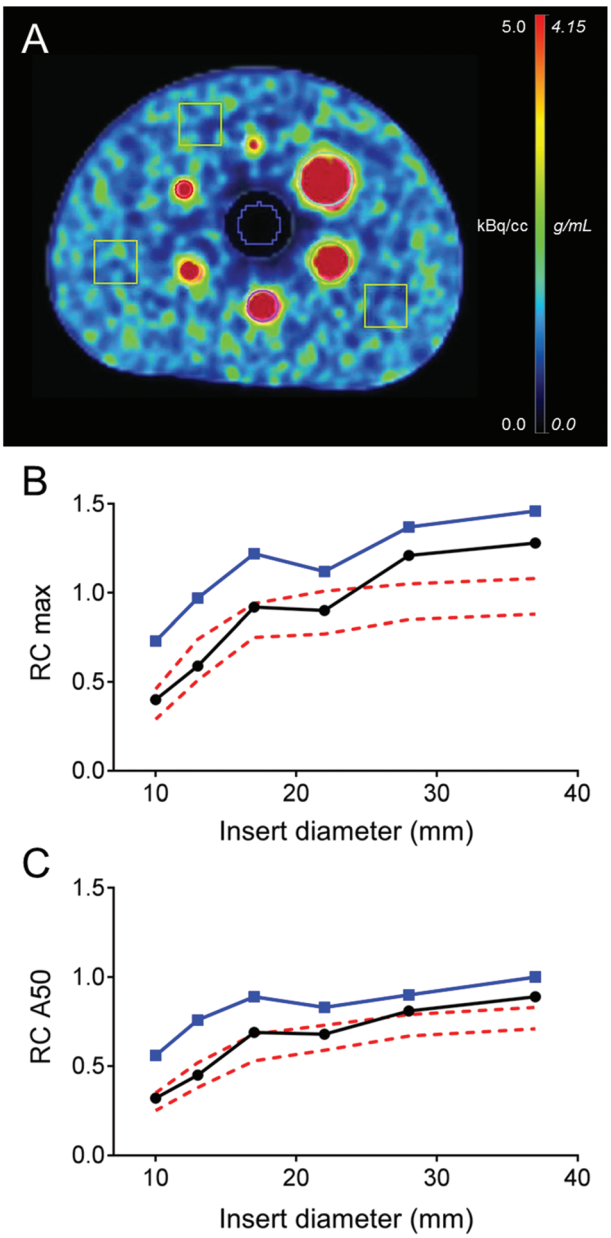

Fig. 1 (A) Transaxial cross section of the NEMA NU2 phantom containing six spherical inserts with diameters of 10 mm, 13 mm, 17 mm, 22 mm, 28 mm and 37 mm, respectively. (B) Relative recovery coefficient (max) and (C) relative recovery coefficient (A50%) as a function of the insert diameter for the TOF (blue full line with squares) and non-TOF (black full line with circles) ^{152}Tb PET/CT reconstruction of the NEMA NU2 phantom. Red dashed lines in the graphs define the range of RC reference values defined by the EANM/EARL for oncological FDG procedures.

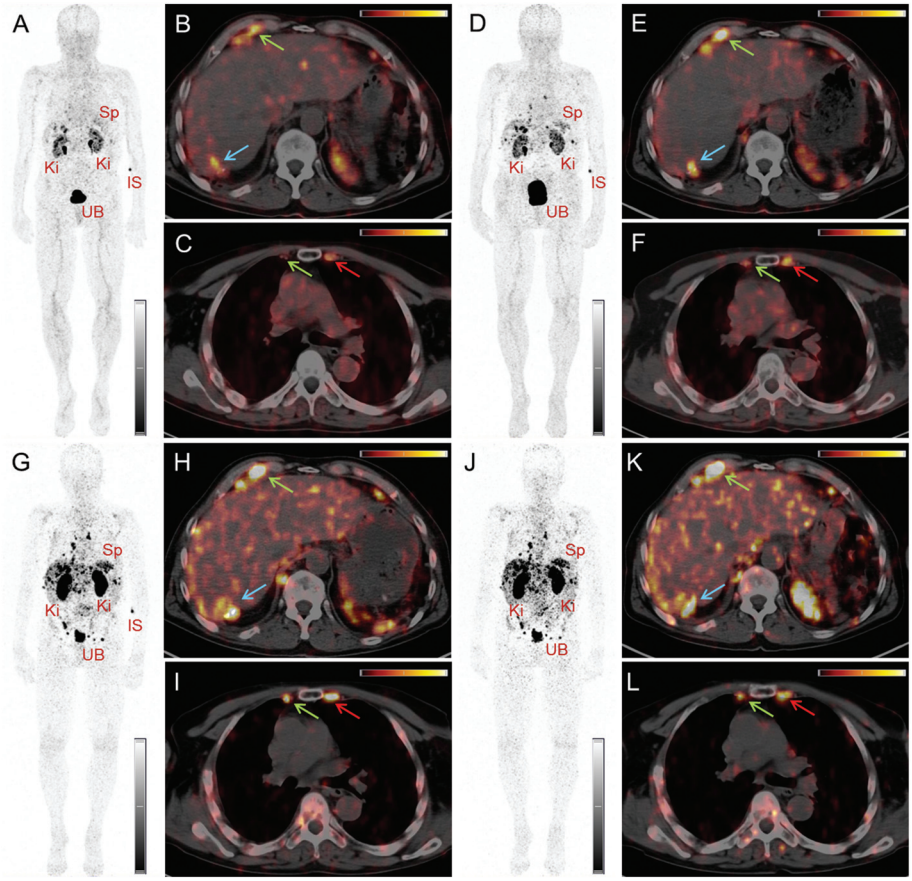

Fig. 2 PET/CT images of a patient with neuroendocrine neoplasm of the terminal ileum obtained at 25 min (A–C), 2 h (D–F), 17 h (G–I) and 24 h (J–L) after injection of ^{152}Tb-DOTATOC, respectively. (A, D, G, J) Maximal intensity projection (MIP) images show the kidneys (Ki), the urinary bladder (UB), the spleen (Sp), and the injection site (IS). (B, C, E, F, H, I, K, L) Transverse sections of PET/CT fusion images demonstrate radiopeptide uptake in lymph node metastases in the right costophrenic region and in the right internal mammary chain (green arrows), as well as in segment 7 of the liver (blue arrows) and in a skeletal metastasis in the left third rib adjacent to the sternocostal junction (red arrows) (UB = urinary bladder; SI = site of injection; Ki = kidneys; Sp = spleen).

spleen, liver, intestines, and kidneys, as well as excreted tracer in the urinary bladder. Even at this delayed time-point, excellent and even increased uptake of the radiopeptide was observed in multiple lymph nodes and skeletal metastases. At all image acquisition time points, the image quality was noisier as compared to ^{68}Ga-based PET scans, which may be attributed to the inability of the software to perform prompt γ-correction for the acquired data.

When compared to the previous PET/CT scans performed with ^{68}Ga-DOTATOC in June 2015 (Fig. 3), all known metastases were visualized and no new metastatic lesions were identified in the PET scan obtained with ^{152}Tb-DOTATOC in May 2016. From a clinical point of view, this (stable disease) was the most important finding of the study.

Discussion

In this study, ^{152}Tb, a novel radionuclide for PET imaging, was used for the first time in a human. The 17.5 h half-life of ^{152}Tb allowed its transport over several hundreds of kilometers across Europe, where it was used for the labeling of DOTATOC and PET/CT imaging of a patient with a neuroendocrine neoplasm. The endeavor involved three widely separated research facilities and hospitals, respectively, where the production, separation, radiolabeling and the administration of the final product, ^{152}Tb-DOTATOC, to a patient was carried out.

The chemical separation of ^{152}Tb from the target material was performed by ion exchange chromatography at PSI. While it is known that labeling is feasible when using ^{152}Tb directly in the eluted α-HIBA elution solution,[11] it was decided to evaporate the liquid and reconstitute the radionuclide in dilute hydrochloric acid to set similar conditions as for commercial radionuclides. That way, efficient radiolabeling of DOTATOC at ZBB for subsequent in-human application was facilitated. By the time the ^{152}Tb product arrived at CHUV and ZBB, respectively, the remaining ^{152}Dy was <0.2% of the ^{152}Tb activity.

The ^{152}Tb PET/CT study with the standard NEMA NU2 phantom showed RC values in agreement with levels typical of clinical ^{18}F- and ^{68}Ga-based PET/CT studies using TOF and

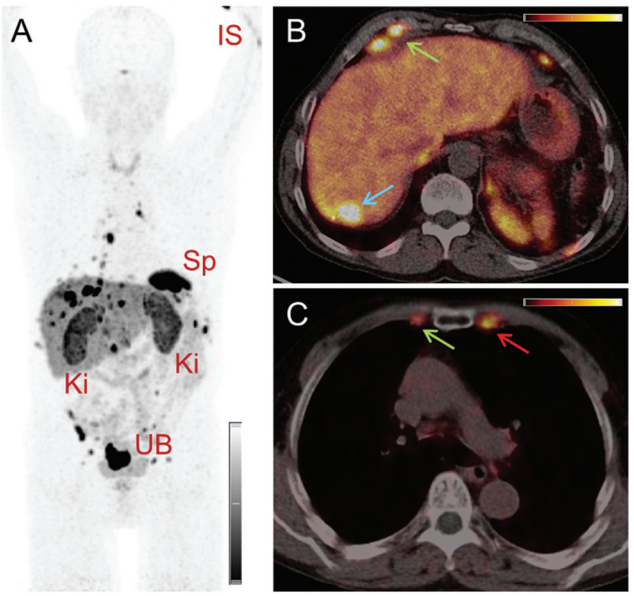

Fig. 3 (A–C) PET/CT images of the same patient acquired 55 min after injection of ^{68}Ga-DOTATOC (104 MBq) 11 months previously. (A) Maximal intensity projection (MIP) images show the kidneys (Ki), the urinary bladder (UB), the spleen (Sp), and the injection site (IS). (B, C) Transverse section of PET/CT fusion images demonstrate lymph node metastases in the right costophrenic region and in the right internal mammary chain (green arrows); uptake is seen in a metastasis in segment 7 of the liver (blue arrow) and in a skeletal metastasis in the left third rib adjacent to the sternocostal junction (red arrow) (UB = urinary bladder; SI = site of injection, Ki = kidneys; Sp = spleen).

PSF corrections.[30] RC values obtained with the simple OSEM3D (no-TOF no-PSF) reconstructions were comparable to PET-derived reference levels reported in the EANM guidelines for oncological ^{18}F-FDG PET protocols. As a consequence, expected signal recovery at matched signal-to-noise ratios in clinical ^{152}Tb-based PET/CT procedures should not be different from the established ^{18}F- and ^{68}Ga-based PET/CT. Particularly high values of maximum RC are explained by the important image noise (COV = 25%). A two-fold increased image noise level was expected because of the smaller β^+ branching ratio of ^{152}Tb ($I\beta^+$ = 20.3%), as compared to ^{18}F ($I\beta^+$ = 97%), at matched activity concentrations and actual frame durations. The signal recovery in the cold region estimated by the relative lung error in the TOF + PSF ^{152}Tb PET/CT reconstruction (ΔC_{lung} = 12.2%) is comparable to the values obtained in TOF + PSF ^{18}F PET/CT.[26] The particularly high value of ΔC_{lung} = 40.2% obtained for the simple OSEM3D reconstruction can be explained by the important signal pollution in the cold lung region consequent to the lack of TOF information and low acquired statistic. At present, the spatial resolution of ^{152}Tb PET/CT imaging was not assessed. This could be done in future experiments using a specifically designed line resolution phantom. The mean energy and the corresponding mean range in tissues of the β^+ emission from ^{152}Tb (1.14 MeV/4.7 mm) are higher than for ^{18}F (0.25 MeV/0.64 mm), but comparable to those for ^{68}Ga (0.836 MeV/3.5 mm).[31] Other studies in which ^{68}Ga was compared to ^{18}F in clinically relevant PET/CT setups did not find relevant differences in terms of resolution and signal recovery.[31,32] According to these studies, which are supported by the results obtained in the current study, the degradation of ^{152}Tb RC as compared to RC values obtained under clinically relevant conditions for ^{18}F- and ^{68}Ga-based PET is not expected.

This first-in-human application of ^{152}Tb-DOTATOC underlined the potential of using ^{152}Tb for PET imaging. The physiological distribution of ^{152}Tb-DOTATOC was similar, but not identical, to the distribution of ^{68}Ga-DOTATOC. This can be attributed to different and delayed PET acquisition time points, as well as the different amounts of the injected peptide (<50 μg for ^{68}Ga, and 150 μg for ^{152}Tb) used for these studies. Moreover, the different coordination chemistry of ^{152}Tb with DOTA as compared to ^{68}Ga may result in slightly different distribution profiles.

In comparison with the ^{68}Ga-based PET scan, the images obtained with ^{152}Tb-DOTATOC were comparatively noisier, which could possibly result from the lack of prompt γ correction of the scatter fractions from photopeaks with γ-energies >511 keV by the current PET software. Visual assessment of the images revealed lower physiological uptake in the pituitary and thyroid glands in comparison with the previous PET/CT scans obtained with ^{68}Ga-DOTATOC. This may be related to the increased amount of peptide injected in the case of ^{152}Tb-DOTATOC as compared to the amount of peptide used for ^{68}Ga-DOTATOC, resulting in lower specific activity. Nonetheless, the PET/CT images acquired using ^{152}Tb-DOTATOC in this study were adequate for diagnostic purposes. In comparison with the PET/CT scan obtained with ^{68}Ga-DOTATOC, all previously detected lymph node, skeletal and liver lesions were clearly identified and there was no evidence of new or progressive metastases. Information of stable disease, which was obtained in this study, was used for making the clinical decision of further follow-up of the patient; therapeutic intervention was not necessary at this stage.

An accurate semi-quantitative assessment of the acquired images using the standard practice of measuring the standard uptake value (SUV) was not feasible for this study, since the software could not be used for calibration of the PET camera for ^{152}Tb. Should this radionuclide be made available for routine clinical use in future, quantification of accumulated activity will be of particular value. A significant advantage of ^{152}Tb over ^{68}Ga is its considerably longer half-life, thus, rendering ^{152}Tb-based PET imaging a potentially valuable tool for pre-therapeutic dosimetry, allowing optimization of the individualized planning of PRRT with either ^{177}Lu- or ^{161}Tb-labeled DOTA-peptides. Terbium and lutetium belong to the group of lanthanides, with almost identical coordination chemistry and, hence, the tissue distribution profile of the corresponding radiolabeled peptides is likely to be the same. This is not the case for ^{68}Ga-labeled peptides, which have different coordination chemistry. The long half-life of ^{152}Tb provides

interesting logistic opportunities, potentially allowing its distribution across Europe and beyond.

Conclusions

This study describes a unique, multi-disciplinary study in which ^{152}Tb was investigated from the production to the first-in-human clinical application. ^{152}Tb was collected *via* a mass separation process, chemically separated and used for phantom studies as well as for the radiolabeling of DOTATOC. The results of the clinical application demonstrated successful PET/CT imaging using ^{152}Tb-DOTATOC in a patient with neuroendocrine neoplasm, allowing the visualization of even small metastases. Due to the considerably longer half-life of ^{152}Tb, as compared to the currently used ^{68}Ga, this novel radionuclide would be particularly interesting for dosimetry prior to radionuclide therapy. While the current availability of ^{152}Tb is limited, the on-going construction of additional ISOL facilities will increase the possibility of pursuing this concept at a larger scale.

Conflicts of interest

There are no conflicts to declare.

Acknowledgements

The authors thank the staff members at the Center for Radiopharmaceutical Sciences at PSI for assistance in the study, as well as the people responsible for radiation safety and radioactive transport for night shifts. The authors are grateful for support by the CERN-ISOLDE teams, in particular the RILIS team and the ISOLTRAP MR-TOF-MS team and thank the radiation safety staff at CERN. The authors would also like to thank Martin Pappon for data acquisition of the phantom study at CHUV, Lausanne, Switzerland. The authors express their gratitude to the physicians, physicists, and nursing staff, as well as the nuclear medicine technologists of the Theranostics Center for Molecular Radiotherapy and Molecular Imaging for patient management at ZBB. This project has received funding from the European Union's Horizon 2020 research and innovation programme under grant agreement no. 654002.

References

1 B. C. Ahn, *BioMed Res. Int.*, 2016, **2016**, 1680464.
2 B. M. Zeglis, J. L. Houghton, M. J. Evans, N. Viola-Villegas and J. S. Lewis, *Inorg. Chem.*, 2014, **53**, 1880–1899.
3 F. Rösch, H. Herzog, B. Stolz, J. Brockmann, M. Köhle, H. Mühlensiepen, P. Marbach and H. W. Müller-Gartner, *Eur. J. Nucl. Med.*, 1999, **26**, 358–366.
4 A. Helisch, G. J. Förster, H. Reber, H. G. Buchholz, R. Arnold, B. Goke, M. M. Weber, B. Wiedenmann, S. Pauwels, U. Haus, H. Bouterfa and P. Bartenstein, *Eur. J. Nucl. Med. Mol. Imaging*, 2004, **31**, 1386–1392.
5 C. J. Anderson and R. Ferdani, *Cancer Biother. Radiopharm.*, 2009, **24**, 379–393.
6 N. A. Smith, D. L. Bowers and D. A. Ehst, *Appl. Radiat. Isot.*, 2012, **70**, 2377–2383.
7 C. Müller, M. Bunka, J. Reber, C. Fischer, K. Zhernosekov, A. Türler and R. Schibli, *J. Nucl. Med.*, 2013, **54**, 2168–2174.
8 C. Müller, M. Bunka, S. Haller, U. Köster, V. Groehn, P. Bernhardt, N. van der Meulen, A. Türler and R. Schibli, *J. Nucl. Med.*, 2014, **55**, 1658–1664.
9 K. Yong and M. Brechbiel, *AIMS Med. Sci.*, 2015, **2**, 228–245.
10 D. Mathe, K. Szigeti, N. Hegedus, I. Horvath, D. S. Veres, B. Kovacs and Z. Szucs, *Appl. Radiat. Isot.*, 2016, **114**, 1–6.
11 C. Müller, K. Zhernosekov, U. Köster, K. Johnston, H. Dorrer, A. Hohn, N. T. van der Walt, A. Türler and R. Schibli, *J. Nucl. Med.*, 2012, **53**, 1951–1959.
12 S. Lehenberger, C. Barkhausen, S. Cohrs, E. Fischer, J. Grunberg, A. Hohn, U. Koster, R. Schibli, A. Turler and K. Zhernosekov, *Nucl. Med. Biol.*, 2011, **38**, 917–924.
13 M. de Jong, W. A. Breeman, B. F. Bernard, E. J. Rolleman, L. J. Hofland, T. J. Visser, B. Setyono-Han, W. H. Bakker, M. E. van der Pluijm and E. P. Krenning, *Eur. J. Nucl. Med.*, 1995, **22**, 608–616.
14 C. Müller, J. Reber, S. Haller, H. Dorrer, P. Bernhardt, K. Zhernosekov, A. Türler and R. Schibli, *Eur. J. Nucl. Med. Mol. Imaging*, 2014, **41**, 476–485.
15 J. Grünberg, D. Lindenblatt, H. Dorrer, S. Cohrs, K. Zhernosekov, U. Köster, A. Türler, E. Fischer and R. Schibli, *Eur. J. Nucl. Med. Mol. Imaging*, 2014, **41**, 1907–1915.
16 S. Haller, G. Pellegrini, C. Vermeulen, N. P. van der Meulen, U. Köster, P. Bernhardt, R. Schibli and C. Müller, *EJNMMI Res.*, 2016, **6**, 13.
17 C. Champion, M. A. Quinto, C. Morgat, P. Zanotti-Fregonara and E. Hindie, *Theranostics*, 2016, **6**, 1611–1618.
18 E. Hindie, P. Zanotti-Fregonara, M. A. Quinto, C. Morgat and C. Champion, *J. Nucl. Med.*, 2016, **57**, 759–764.
19 S. Koukouraki, L. G. Strauss, V. Georgoulias, J. Schuhmacher, U. Haberkorn, N. Karkavitsas and A. Dimitrakopoulou-Strauss, *Eur. J. Nucl. Med. Mol. Imaging*, 2006, **33**, 460–466.
20 A. R. Haug, R. Cindea-Drimus, C. J. Auernhammer, M. Reincke, B. Wangler, C. Uebleis, G. P. Schmidt, B. Goke, P. Bartenstein and M. Hacker, *J. Nucl. Med.*, 2012, **53**, 1686–1692.
21 L. Peter, J. Sanger, M. Hommann, R. P. Baum and D. Kaemmerer, *Clin. Nucl. Med.*, 2014, **39**, 713–716.
22 P. Sharma, S. Arora, A. Mukherjee, S. Pal, P. Sahni, P. Garg, R. Khadgawat, S. Thulkar, C. Bal and R. Kumar, *Clin. Nucl. Med.*, 2014, **39**, 37–43.
23 C. Müller, C. Vermeulen, K. Johnston, U. Köster, R. Schmid, A. Türler and N. P. van der Meulen, *EJNMMI Res.*, 2016, **6**, 35.

24 B. J. Allen, G. Goozee, S. Sarkar, G. Beyer, C. Morel and A. P. Byrne, *Appl. Radiat. Isot.*, 2001, **54**, 53–58.
25 U. Köster, *Nucl. Phys. A*, 2002, **701**, 441c–451c.
26 V. Bettinardi, L. Presotto, E. Rapisarda, M. Picchio, L. Gianolli and M. C. Gilardi, *Med. Phys.*, 2011, **38**, 5394–5411.
27 R. Boellaard, N. C. Krak, O. S. Hoekstra and A. A. Lammertsma, *J. Nucl. Med.*, 2004, **45**, 1519–1527.
28 V. Rosslyn, *The Association of Electrical Equipment and Medical Imaging Manufacturers*, 2007.
29 R. N. Wolf, D. Beck, K. Blaum, C. Bohm, C. Borgmann, M. Breitenfeldt, F. Herfurth, A. Herlert, M. Kowalska, S. Kreim, D. Lunney, S. Naimi, D. Neidherr, M. Rosenbusch, L. Schweikhard, J. Stanja, F. Wienholtz and K. Zuber, *Nucl. Instr. Meth. A*, 2012, **686**, 82–90.
30 E. Quak, P. Y. Le Roux, M. S. Hofman, P. Robin, D. Bourhis, J. Callahan, D. Binns, C. Desmonts, P. Y. Salaun, R. J. Hicks and N. Aide, *Eur. J. Nucl. Med. Mol. Imaging*, 2015, **42**, 2072–2082.
31 A. T. Soderlund, J. Chaal, G. Tjio, J. J. Totman, M. Conti and D. W. Townsend, *J. Nucl. Med.*, 2015, **56**, 1285–1291.
32 P. Kench, N. Forwood, K. Willowson and D. Bailey, *J. Nucl. Med.*, 2013, **54**, 2121.